

Secondary Organic Aerosol Formation during the Photo-Oxidation of Toluene: Dependence on Initial Hydrocarbon Concentration

Kei Sato,[1] Björn Klotz,[1,†] Shiro Hatakeyama,[1] Takashi Imamura,*[,1] Yuuki Washizu,[2] Yutaka Matsumi,[2] and Nobuaki Washida[3]

[1]National Institute for Environmental Studies, Tsukuba, Ibaraki 305-8506

[2]Solar-Terrestrial Environment Laboratory, Nagoya University, Toyokawa, Aichi 442-8507

[3]Department of Chemistry, Graduate School of Science, Kyoto University, Sakyo-ku, Kyoto 606-8502

Received August 11, 2003; E-mail: imamura@nies.go.jp

Aerosol formation in toluene–NO_x–air–photoirradiation systems was examined in a 6-m^3 photochemical reaction chamber. The initial toluene concentration was varied between 2 and 16 ppmv, whereas the initial NO_x concentration was kept constant. The aerosol mass concentrations were plotted as a function of the concentration of toluene reacted. The aerosol profiles showed a curved feature at low toluene consumptions, and merged into a single line at longer reaction times. The observed characteristics were explained by assuming condensable products were formed through reactions of ozone with primary toluene photo-oxidation products.

Aromatic hydrocarbons (AHCs) are an important class of organic compounds in urban air, and their atmospheric oxidation is believed to contribute to the formation of secondary organic aerosol as well as photochemical ozone.[1] Laboratory experiments have shown that the aerosol yields for an individual organic compound depend on several factors, and that a single compound does not form aerosol in a constant yield.[2–5] Odum et al.[6] analyzed the measured aerosol yields on the basis of a gas–particle partitioning absorption model and interpreted the yield data as a function of the organic aerosol mass concentration. However, the expressions for aerosol yield in terms of aerosol mass concentration provide little information on the reaction mechanisms leading to the formation of organic aerosol. It should be possible, however, to determine the mechanism of aerosol formation by analysis of aerosol profiles as a function of reaction time or the concentration of the precursor species.

Aerosol formation from AHCs in most smog chamber experiments was characterized by a delay in the timing of aerosol formation. That is, the aerosol was detected only after photochemical ozone was formed. Izumi and Fukuyama[7] pointed out that, in the AHC–NO_x–air photoirradiation system, the amount of AHC lost before the aerosol was detected was not affected by the replacement of NO by NO_2 in the initial reaction mixture, and concluded that the aerosol was not produced directly from AHC but secondarily from the gaseous products. Bowman et al.[8] applied a dynamic model for the gas–particle absorptive partitioning of semi-volatile organic aerosol to simulate aerosol profiles from *m*-xylene. They demonstrated that the timing of aerosol formation was delayed when the semi-volatile compounds were products of secondary instead of primary reactions, and concluded that the condensing species from *m*-xylene were second- rather than first-generation products of the photo-oxidation. Hurley et al.[9] found that the aerosol profiles during the atmospheric oxidation of toluene could be divided into two groups—aerosol formed in the absence of ozone and aerosol formed in the presence of ozone—and suggested that the reactions of OH radicals, NO_3 radicals, and/or ozone with the first-generation products of toluene oxidation were sources of condensable products.

However, it is still unclear whether aerosol formation from AHCs is the result of OH radical, ozone, or NO_3 radical reactions, assuming the condensable species are products of secondary reactions. In this work, we focused on aerosol formation from toluene because toluene is the simplest reactive AHC. Aerosol concentration profiles were determined for different initial toluene concentrations, while the initial NO_x concentration was kept constant. This experimental protocol was chosen because, under our experimental conditions, the maximum concentration of photochemically-generated ozone was almost independent of the initial toluene concentration, whereas the OH radical concentration decreased with increasing toluene concentration. The observed profiles were analyzed with a box model using simple reaction schemes.

Experimental

Experiments were conducted in a 6-m^3 evacuable and bakeable chamber whose inner surface was coated with perfluoroethylene-perfluoroalkyl vinyl ether copolymer. The details of the apparatus are described elsewhere.[10,11] The chamber was filled with 1 atm of purified air prior to each experiment. The toluene, NO, and CH_3ONO reactants at the desired partial pressures were introduced into calibrated bulbs and then flushed into the chamber with pure N_2 carrier gas. The photolysis of CH_3ONO in the presence of NO was used as an initial source of OH radical. The mixture was irradiated with a solar simulator consisting of nineteen 1-kW Xe arc lamps. The photodissociation rate constant of NO_2 was $(4.0 \pm 0.2) \times 10^{-3}$ s^{-1}. The reaction mixture was stirred well with

† Present address: Cognis Deutschland GmbH & Co KG, Henkelstrasse 67, D-40551 Düsseldorf, Germany

Published on the web April 2, 2004; DOI 10.1246/bcsj.77.667

a mixing fan prior to the photoirradiation. The concentrations of gaseous reactants and products were measured every 6 min with an FT-IR spectrometer (Nicolet Nexus 670) combined with a multi-reflection mirror system (optical path length = 221.5 m). The spectral resolution was 1.0 cm^{-1}. Aerosol particle distributions were measured with a scanning mobility particle sizer instrument (TSI Model 3934) consisting of an electrostatic classifier (TSI Model 3071A) and a condensation particle counter (TSI Model 3022A). The aerosols were sampled through a 1/4-in-diameter × 60-cm-long stainless steel tube at a flow rate of 0.4 L min^{-1}. The wall deposition rates of aerosol were measured by monitoring the aerosol concentration in the dark after conclusion of the experiments. An excess of NO was introduced to suppress further ozone and NO_3 radical reactions in the dark. The typical decay rate of the aerosol volume was ca. 0.005 min^{-1}. Corrections for this wall deposition were applied to all aerosol volume concentrations. All experiments were carried out in the absence of seed particles at 101 ± 1 kPa of dry air and 298 ± 2 K.

Results and Discussion

The time profile of the organic aerosol mass concentration during photoirradiation of the toluene–NO–CH_3ONO–air system is shown in Fig. 1a. The aerosol mass concentration (μg m^{-3}), [aerosol], was calculated from the electrical mobility diameter, assuming a spherical shape and a density of 1 g cm^{-3}. The initial concentrations of toluene, NO, and CH_3ONO were

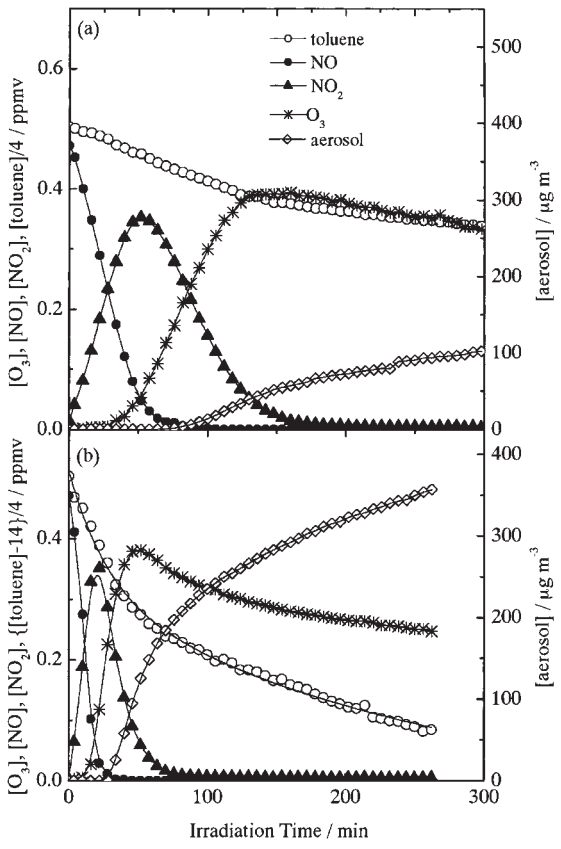

Fig. 1. Observed concentrations of toluene, NO, NO_2, O_3, and aerosol as a function of irradiation time. The initial concentration of toluene was (a) 2.0 and (b) 16 ppmv. The initial concentrations of NO and CH_3ONO were 0.47 and 0.03 ppmv, respectively, for both experiments.

$[toluene]_0 = 2.0$, $[NO]_0 = 0.47$, and $[CH_3ONO]_0 = 0.03$, all in units of ppmv. The time profiles for the toluene, NO, NO_2, and O_3 are also plotted in the figure. The maximum concentration of ozone reached 394 ppbv. The aerosol appeared when the ozone production rate, $d[O_3]/dt$, was at nearly the maximum. Once the aerosol formed, its mass concentration increased with increasing irradiation time. Figure 1b shows the results for an experiment with $[toluene]_0 = 16$ ppmv. $[NO]_0$ and $[CH_3ONO]_0$ were fixed at 0.47 and 0.03 ppmv, respectively. The maximum ozone concentration, $[O_3]_{max}$, reached 382 ppbv. Although the induction period for aerosol formation was shorter than in Fig. 1a, in this experiment, aerosol formation started when $d[O_3]/dt$ was at almost its maximum, as also for $[toluene]_0 = 2$ ppmv. Once the aerosol formed, the aerosol mass concentration increased sharply. Similar experiments were carried out at $[toluene]_0 = 4$ and 8 ppmv. $[O_3]_{max}$ was insensitive to $[toluene]_0$, as expected ($[O_3]_{max} = 393$ ppbv for $[toluene]_0 = 4$ ppmv, $[O_3]_{max} = 388$ ppbv for $[toluene]_0 = 8$ ppmv). In these experiments, the characteristics of aerosol formation were similar to those in Fig. 1: the induction period of aerosol formation became shorter and the increase in aerosol concentration became more rapid with increasing $[toluene]_0$.

A plot of the aerosol mass concentration as a function of the concentration of toluene reacted, Δ[toluene] (Fig. 2), suggests that a Δ[toluene] threshold, $\Delta[toluene]_{th}$, for aerosol formation exists and that higher values of $[toluene]_0$ lead to higher values of $\Delta[toluene]_{th}$. Above $\Delta[toluene]_{th}$, the aerosol mass concentration increases with increasing Δ[toluene], and each profile shows a curved feature. That is, d[aerosol]/dΔ[toluene] increases with increasing Δ[toluene]. The curved feature is most pronounced in the experiment with the highest $[toluene]_0$. After a sufficient amount of toluene was consumed, the aerosol concentration appeared to increase linearly with increasing Δ[toluene]. Furthermore, the aerosol concentration in all the experiments appeared to merge into a single straight line, as shown by the dashed line in Fig. 2, regardless of $[toluene]_0$.

The aerosol profiles were analyzed by assuming the following simple reaction schemes.

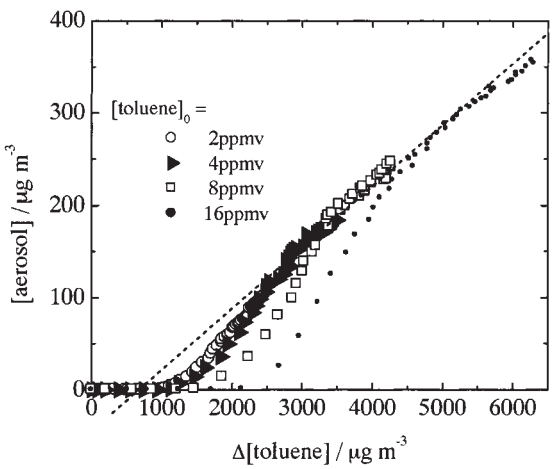

Fig. 2. Aerosol mass concentrations from the photo-oxidation of toluene as a function of toluene consumption. The dashed line qualitatively shows the merging of the aerosol concentrations into a single line.

I: Direct production of a condensable product P_1 from toluene.

$$\text{Toluene} + \text{OH} \rightarrow P_1(g) + \text{other products:} \quad k_1 \qquad (1)$$

$$P_1(g) \rightarrow P_1(a).$$

II: Secondary production of a condensable product S_1 through the reaction of OH radicals with a primary product P_2.

$$\text{Toluene} + \text{OH} \rightarrow P_2(g) + \text{other products}$$

$$P_2(g) + \text{OH} \rightarrow S_1(g) + \text{other products:} \quad k_2 \qquad (2)$$

$$S_1(g) \rightarrow S_1(a).$$

III: Secondary production of a condensable product S_2 through the reaction of O_3 with the primary product P_2.

$$P_2(g) + O_3 \rightarrow S_2(g) + \text{other products:} \quad k_3 \qquad (3)$$

$$S_2(g) \rightarrow S_2(a).$$

Here, k_i is the second-order rate constant for reaction (i). X(g) and X(a) represent the species X in the gas and aerosol phases, respectively, and P_i and S_i represent the primary and secondary products, respectively. The yields of primary products P_1 and P_2 during the toluene oxidation by OH radicals and those of secondary products S_1 and S_2 in reactions 2 and 3 are assumed to be constant in the calculations. The total concentration of species X, $[X]_{tot}$, is the sum of the concentrations in the gas and aerosol phases, $[X]_g$ and $[X]_a$. These simplified reaction schemes were employed in box model calculations to determine which scheme best fits the observed aerosol profiles. In the calculations, the experimental concentrations of toluene and ozone were used. The OH radical concentrations were derived from the time profiles for toluene and the reported rate constant for the OH + toluene reaction, 6.0×10^{-12} cm^3 molecule^{-1} s^{-1}.[12] In our calculations, we assumed that once the concentration of the condensable species X exceeds its saturation level, $[X]_{sat}$, X starts forming aerosol; that is, $[X]_a = [X]_{tot} - [X]_{sat}$ for $[X]_{tot} \geq [X]_{sat}$ and $[X]_a = 0$ for $[X]_{tot} < [X]_{sat}$.

In Fig. 3, the total calculated concentrations of condensable products (P_1 for reaction scheme I, S_1 for reaction scheme II, and S_2 for reaction scheme III) are plotted as a function of Δ[toluene]. The dashed lines in the figure represent the saturation levels of P_1, S_1, and S_2 that fit the $\Delta[\text{toluene}]_{th}$ in the experiment with $[\text{toluene}]_0 = 4$ ppmv. The calculations based on reaction scheme I predict that the total concentration of P_1 is directly proportional to Δ[toluene], regardless of $[\text{toluene}]_0$, and $\Delta[\text{toluene}]_{th}$ is also independent of $[\text{toluene}]_0$ (Fig. 3a). Reaction scheme I clearly fails to reproduce the characteristics of the experimental aerosol profiles.

Reaction scheme II is essentially the same as the reactions considered by Hurley et al.[9] The calculations based on reaction scheme II show that lower values of $[\text{toluene}]_0$ lead to lower values of $\Delta[\text{toluene}]_{th}$ and higher values of $[S_1]_{tot}$ (Fig. 3b). This reflects the fact that fewer OH radicals are available for reaction 2 because the higher $[\text{toluene}]_0$ acts as a sink for the radicals.[9] In this calculation, the rate constant for reaction 2 was assumed to be 1×10^{-11} cm^3 molecule^{-1} s^{-1}. The result obtained with reaction scheme II qualitatively explains the curved

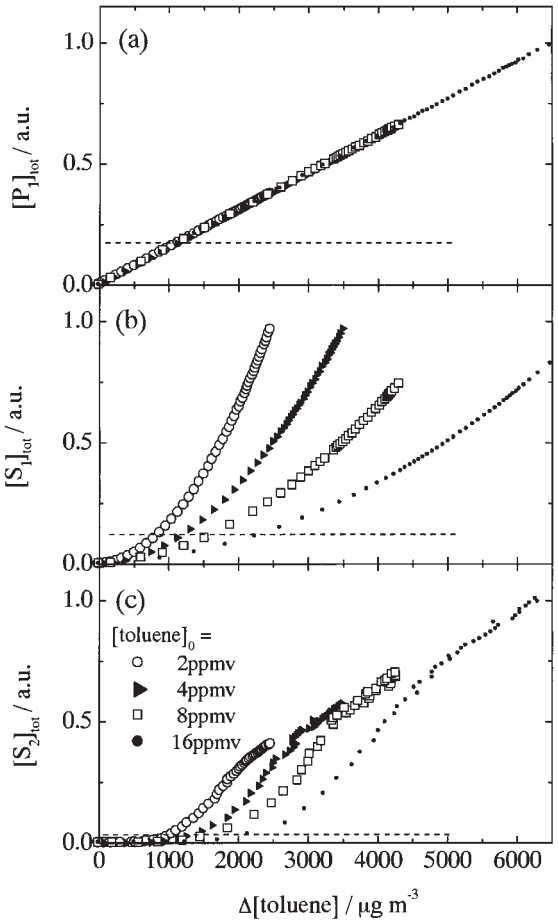

Fig. 3. Calculated total concentrations of condensable products (a) P_1, (b) S_1, and (c) S_2 as a function of the concentration of toluene reacted, as derived from reaction schemes I, II, and III, respectively. The dashed lines show the saturation level of condensable products P_1, S_1, and S_2 that reproduce the threshold concentration of toluene for aerosol formation observed in the experiment with $[\text{toluene}]_0 = 4$ ppmv.

feature of the aerosol profiles in the early stage of aerosol formation. However, our calculation predicts that, when a sufficient amount of toluene reacts above the threshold, the aerosol mass concentration is higher for a lower $[\text{toluene}]_0$. This is not consistent with the experimental profiles, which merge into a single line (Fig. 2). Changing the value of k_2 from 1×10^{-12} to 1×10^{-10} cm^3 molecule^{-1} s^{-1} results in an earlier transition of the $[S_1]_{tot}$ profiles from a curved to a linear response, as discussed by Hurley et al.,[9] but does not explain the difference between the calculated $[S_1]_{tot}$ profiles and the experimental aerosol profiles.

The total concentration of S_2, $[S_2]_{tot}$, calculated on the basis of reaction scheme III is plotted as a function of Δ[toluene] in Fig. 3c. In calculating $[S_2]_{tot}$, we set the rate constant for reaction 3 to 5×10^{-17} cm^3 molecule^{-1} s^{-1}. Apparently, S_2 is produced after some toluene is consumed and $\Delta[\text{toluene}]_{th}$ for the production of S_2 increases as $[\text{toluene}]_0$ increases. The existence of a threshold for the production of S_2 simply reflects the fact that a certain amount of toluene is consumed before ozone is formed. The dependence of $\Delta[\text{toluene}]_{th}$ on $[\text{toluene}]_0$

is due to the fact that more toluene is consumed prior to O_3 formation at higher $[toluene]_0$ than at lower $[toluene]_0$. At higher initial concentrations, toluene is a more efficient OH radical scavenger, leading to faster degradation of toluene. Once S_2 is generated, $d[S_2]_{tot}/d\Delta[toluene]$ is expected to increase with increasing $\Delta[toluene]$ in the early stage of S_2 production, when the ozone concentration rises sharply. The curved feature of the calculated $[S_2]$ profiles is more pronounced for higher $[toluene]_0$, as in the experimental aerosol profiles. This reflects the fact that the ozone formation efficiency, $d[O_3]/d\Delta[toluene]$, decreases with increasing $[toluene]_0$, whereas the amount of P_2 accumulated before ozone formation increases. The $[S_2]_{tot}$ profiles calculated for four different $[toluene]_0$ conditions merge into a single line, as in the experimental aerosol profiles. This feature can be explained as follows: after most of the P_2 accumulated before ozone formation is converted to S_2 by reaction 3, the production rate of S_2 is controlled by the production of P_2 from toluene rather than the conversion of P_2 to S_2, because the high concentration of ozone and relatively large value of k_3 make the lifetime of P_2 short. Therefore, the efficiency of S_2 production as a function of the loss of toluene, $d[S_2]/d\Delta[toluene]$, becomes independent of $[toluene]_0$. The features of the calculated profiles were sensitive to the value of k_3. For example, a model calculation with $k_3 = 5 \times 10^{-18}$ cm^3 $molecule^{-1}$ s^{-1} did not reproduce the part of the profile that merged into a single line because, on the experimental time scale, the value of k_3 is not large enough to convert the P_2 produced before ozone formation to S_2.

Another chemical species that can oxidize the primary product P_2 is the NO_3. NO_3 radicals can react with some of the primary products of toluene rather than with toluene itself. For example, the rate constants for the reactions of NO_3 radicals with toluene and *o*-cresol (one of the oxidation products of toluene) are 7×10^{-17} and 4×10^{-11} cm^3 $molecule^{-1}$ s^{-1}, respectively.[13] The oxidation products from the reaction of P_2 with NO_3 radicals might contribute to aerosol formation.

$$P_2(g) + NO_3 \rightarrow S_3(g) + \text{other products} \quad (4)$$

$$S_3(g) \leftrightarrow S_3(a)$$

In this work, NO_3 radicals were produced by the reaction of NO_2 with ozone,

$$NO_2 + O_3 \rightarrow NO_3 + O_2 \quad (5)$$

which would also lead to a latent consumption of toluene before the condensable product is formed in sufficient amount to form aerosol. However, because the concentration-time profile for NO_3 is expected to be different from that for O_3, and the concentration of NO_3 radicals should be high in the limited time region when both $[NO_2]$ and $[O_3]$ are high,[14] the $[S_3]_{tot}$ profiles should be distinctly different from the $[S_2]_{tot}$ profiles. Specifically, they should not merge into a straight line. A preliminary $[S_3]_{tot}$ calculation did not reproduce the experimental aerosol profiles as well as the $[S_2]_{tot}$ calculation shown in Fig. 3c.

The aerosol profile and its $[toluene]_0$ dependence were analyzed by assuming these three simple reaction schemes. This analysis suggested that the reaction of O_3 with the primary product P_2 from toluene plays an important role in aerosol formation. The characteristics of the experimental aerosol profiles can be explained by rapid conversion of the primary product P_2 into the condensable product S_2 by O_3, the production of which requires the latent consumption of toluene.

The second-order rate constant of the OH + propene reaction (2.6×10^{-11} cm^3 $molecule^{-1}$ s^{-1})[15] is larger than k_1, and photo-oxidation of propene in the presence of NO_x produces a higher concentration of ozone than toluene does.[16] However, the photo-oxidation products of propene are not expected to contribute to aerosol formation. Therefore, the effect of the presence of propene on aerosol formation from toluene would be a good test for the reaction scheme. Aerosol formation experiments were conducted in the presence and in the absence of 4 ppmv of propene (Fig. 4). The initial concentrations of toluene, NO, and CH_3ONO were fixed at 8.0, 0.47, and 0.03 ppmv, respectively. The presence of propene led to a reduction in the latent consumption of toluene for aerosol formation and a slight decrease in $d[aerosol]/d\Delta[toluene]$ (Fig. 4). Box model calculations based on reaction scheme III were performed for the reactions with propene (Fig. 4, broken line) and without propene (Fig. 4, continuous line). The experimental profiles could be reproduced by a calculation with the same saturation level of S_2. The characteristics of the aerosol profiles could largely be explained in terms of the variation of ozone concentration. These results support the importance of the O_3 reaction in aerosol formation.

As discussed above, secondary reactions of O_3 with the primary oxidation products from toluene play an important role in aerosol formation. A good way to check this result is to determine the molecular composition of the aerosol. From studies of the molecular composition of aerosol formed during the photo-oxidation of toluene, Forstner et al.[17] suggested that condensable components were produced through photolysis and/or reactions with OH radicals of the primary toluene photo-oxidation products. However, the identified components[17] of aerosol are

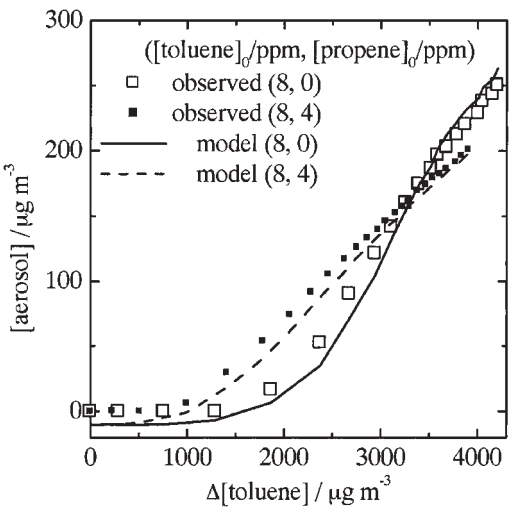

Fig. 4. Aerosol mass concentrations vs the concentration of toluene reacted in the presence (open squares) and absence (solid squares) of 4 ppmv of propene. The initial concentration of toluene was 8 ppmv. The broken and continuous lines are the results of the box model calculations based on reaction scheme III in the experiments with and without propene, respectively.

semi-volatile and their concentrations would not exceed their saturation levels in our experiments. Furthermore, it can not be safely ruled out that the O_3 and/or NO_3 reactions influenced aerosol formation, because these composition measurements[17] were carried out under the conditions of a relatively high initial NO_x concentration, $\geq$0.9 ppmv. Thus, reliable composition measurements including non-volatile components under defined conditions are needed.

In summary, secondary organic aerosol formation from toluene was observed with different initial toluene concentrations with constant NO_x concentration. Curved [aerosol] vs Δ[toluene] profiles were obtained during the early stage of aerosol formation. At higher toluene consumptions, the aerosol profiles merged into a single line. The former characteristic became more pronounced with increasing $[\text{toluene}]_0$, whereas the latter characteristic was insensitive to $[\text{toluene}]_0$. These characteristics could be explained when condensable products were assumed to be formed through reactions of ozone with primary toluene photo-oxidation products. Measurements of aerosol formation as a function of $[NO_x]_0$ would be a good test for the proposed mechanism because the ozone concentration depends on $[NO_x]_0$. Such measurements are now in progress.

B. K. gratefully acknowledges successive fellowships from the Japan Science and Technology Agency (STA)/Alexander von Humboldt Foundation and the Ministry of the Environment. This work was supported by a Grant-in-Aid for Scientific Research from the Ministry of Education, Culture, Sports, Science and Technology and a Global Environment Research Fund Project from the Ministry of the Environment.

References

1 J. R. Odum, T. P. W. Jungkamp, R. J. Griffin, R. C. Flagan, and J. H. Seinfeld, *Science*, **276**, 96 (1997).

2 J. A. Leone, R. C. Flagan, D. Grosjean, and J. H. Seinfeld, *Int. J. Chem. Kinet.*, **17**, 177 (1985).

3 J. E. Stern, R. C. Flagan, D. Grosjean, and J. H. Seinfeld, *Environ. Sci. Technol.*, **21**, 1224 (1987).

4 S. N. Pandis, S. E. Paulson, J. H. Seinfeld, and R. C. Flagan, *Atmos. Environ.*, **25A**, 997 (1991).

5 K. Izumi, K. Murano, M. Mizuochi, and T. Fukuyama, *Environ. Sci. Technol.*, **22**, 1207 (1988).

6 J. R. Odum, T. P. W. Jungkamp, R. J. Griffin, H. J. L. Forstner, R. C. Flagan, and J. H. Seinfeld, *Environ. Sci. Technol.*, **31**, 1890 (1997).

7 K. Izumi and T. Fukuyama, *Atmos. Environ.*, **24A**, 1433 (1990).

8 F. M. Bowman, J. R. Odum, J. H. Seinfeld, and S. N. Pandis, *Atmos. Environ.*, **23**, 3921 (1997).

9 M. D. Hurley, O. Sokolov, T. J. Wallington, H. Takekawa, M. Karasawa, B. Klotz, I. Barnes, and K. H. Becker, *Environ. Sci. Technol.*, **35**, 1358 (2001).

10 H. Akimoto, M. Hoshino, G. Inoue, F. Sakamaki, N. Washida, and M. Okuda, *Environ. Sci. Technol.*, **13**, 471 (1979).

11 S. Hatakeyama, T. Imamura, and N. Washida, *Bull. Chem. Soc. Jpn.*, **72**, 1497 (1999).

12 R. Atkinson, *J. Phys. Chem. Ref. Data, Monograph No. 1*, **1989**, 1.

13 J. G. Calvert, R. Atkinson, K. H. Becker, R. M. Kamens, J. H. Seinfeld, T. J. Wallington, and G. Yarwood, "The Mechanisms of Atmospheric Oxidation of Aromatic Hydrocarbons," Oxford University Press, Oxford, U. K. (2002).

14 B. Klotz, S. Sørensen, I. Barnes, K. H. Becker, T. Etzkorn, R. Volkamer, U. Platt, K. Wirtz, and M. Martín-Reviejo, *J. Phys. Chem. A*, **102**, 10289 (1998).

15 R. Atkinson, *J. Phys. Chem. Ref. Data*, **26**, 215 (1997).

16 F. Sakamaki and H. Akimoto, *Environ. Sci. Technol.*, **17**, 762 (1983).

17 H. J. L. Forstner, R. C. Flagan, and J. H. Seinfeld, *Environ. Sci. Technol.*, **31**, 1345 (1997).